Available online at www.sciencedirect.com

ScienceDirect

Mendeleev Commun., 2024, **34**, 382–384

Mendeleev Communications

Structure and properties of the metal-containing monomer based on nickel acrylate and 4′-phenyl-2,2′:6′,2″-terpyridine for self-healing polymers

Evgeny S. Sorin,*[a] Rose K. Baimuratova,[a] Valery V. Tkachev,[a] Andrey N. Utenyshev,[a] Alexey V. Kuzmin[b] and Gulzhian I. Dzhardimalieva*[a,c]

[a] *Federal Research Center of Problems of Chemical Physics and Medicinal Chemistry, Russian Academy of Sciences, 142432 Chernogolovka, Moscow Region, Russian Federation. E-mail: sorin_es@mail.ru; dzhardim@icp.ac.ru*

[b] *Institute of Solid State Physics, Russian Academy of Sciences, 142432 Chernogolovka, Moscow Region, Russian Federation*

[c] *Moscow Aviation Institute (National Research University), 125993 Moscow, Russian Federation*

DOI: 10.1016/j.mencom.2024.04.022

A new complex of nickel acrylate and 4′-phenyl-2,2′:6′,2″-terpyridine, analogs of which have been previously used to obtain self-healing metallopolymers, has been prepared. The complex was analyzed by X-ray diffraction, IR and UV absorption spectroscopy, differential scanning calorimetry and thermogravimetric analysis. The values of effective activation energy of solid-phase polymerization and heat of double bond opening for this complex have been calculated.

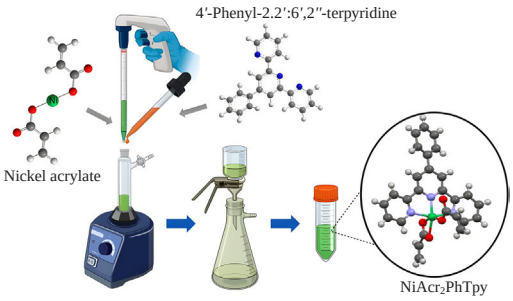

Keywords: terpyridine, metal acrylates, nickel complexes, unsaturated complexes, crystal structure, self-healing.

Metal–ligand coordination is one of the most important interactions in supramolecular chemistry. In terms of creating self-organizing structures *via* self-assembly processes, terpyridines and their derivatives have been actively used in the last two decades. The manifestation of tridentate properties with the formation of dendrimeric terpyridine ligands makes it possible to produce metal-containing polymers used as various sensors.[1–5] An interesting emerging field is the development of terpyridine antitumor agents.[6–10] Besides, terpyridine derivatives can be applied in photodynamic therapy.[11,12] The redox and photophysical properties of various terpyridine architectures allow one to use them in the design of LEDs and LECs.[13–15] The application of terpyridines in catalysis is also known.[16,17]

Currently, a large number of works are devoted to the creation of smart materials with shape memory and self-healing properties.[18–21] Functionalization of polymer chains with terpyridine ligands allows one to obtain self-healing metallopolymers due to the inclusion of reversible metal–ligand coordination interactions.[22] The initial approach to the creation of such systems was to impregnate terpyridine-containing polymers with salts of various transition metals.[23] Thus, it was possible to obtain self-healing systems with an internal healing mechanism due to reversible interactions, but metallopolymers produced in this way often lacked the ability of autonomous healing (occurring without the influence of temperature or irradiation), as well as high-strength characteristics.

Previously,[24–26] we proposed a new one-step protocol for the preparation of new types of self-healing copolymers of acrylamide, acrylic acid and mixed-ligand metal chelate monomers (MCMs) functionalized with 4′-phenyl-2,2′:6′,2″-terpyridine. The incorporation of the metal-containing monomer directly into the polymer chain, as well as the absence of an impregnation step of the final polymer product, significantly improve the mechanical properties of the final polymer films and also allow for autonomous internal healing. Hence, it is of interest to expand this type of MCMs.

This work is devoted to the synthesis and investigation of the complex of nickel acrylate with 4′-phenyl-2,2′:6′,2′-terpyridine. The structure of the complex and its analysis, activation energies of solid-phase polymerization and heat of double bond opening, the values of which can affect the final composition, structure and properties of self-healing polymers, are presented.

Crystallographic data and main refinement parameters for the obtained complex are given in Tables S1–S5 (Online Supplementary Materials), the general appearance of the compound is shown in Figure 1.[†] The Ni^{II} ion has a coordination

[†] *Crystal data for* $NiAcr_2PhTpy$. $C_{27.50}H_{22.50}Cl_{1.50}N_3NiO_{4.50}$ (M = 578.87), at 273.15 K, triclinic, $P\bar{1}$ (2), a = 8.464(2), b = 10.921(2) and c = 14.882(3) Å, α = 98.04(3), β = 94.65(3) and γ = 105.43(3)°, V = 1302.9(5) Å^3, Z = 2, μ = 0.940 mm^{-1}; reflections collected = 5119; final R indices [$I > 2\sigma(I)$]: R_1 = 0.0921, wR_2 = 0.2501; R indexes (all data): R_1 = 0.0983 and wR_2 = 0.2576.

X-ray diffraction studies were carried out on single crystals on an Agilent XCalibur CCD diffractometer with EOS detector. Data acquisition and processing, determination and refinement of unit cell parameters were performed in the CrysAlis PRO program.[27] The structure was solved by dual methods using SHELXT and refined by full-matrix least-squares methods against F^2 by SHELXL using Olex2.[28–30] All non-

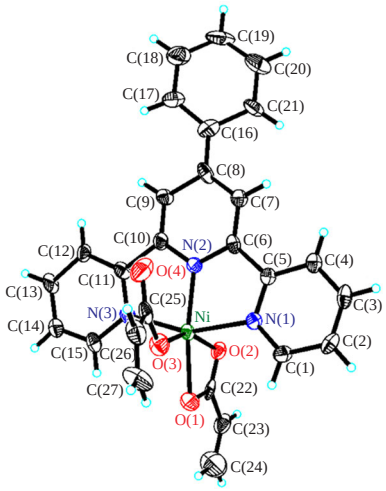

Figure 1 General view of the complex of nickel acrylate and 4′-phenyl-2,2′:6′,2″-terpyridine ($NiAcr_2PhTpy$) without solvent molecule.

number of 6. The coordination sphere is formed by three nitrogen and three oxygen atoms with the following bond lengths (Å): Ni–N(1), 2.096(5); Ni–N(2), 1.980(5); Ni–N(3), 2.072(6); Ni–O(1), 2.112(5); Ni–O(2), 2.186(5); Ni–O(3), 1.989(5). The acrylic acid anions involved in the complexation are differently coordinated with regard to the Ni^{II} ion. One anion acts as a bidentate ligand and the other is coordinated as a monodentate one. The difference in C–O bond lengths is much smaller in the carboxylate group of the bidentate ion compared to the monodentate ion, which is caused by delocalization of electron density and relative alignment of O(1)–C(22) and O(2)–C(22) bonds. The O(4)–C(25) bond in the monodentate anion is double. Account should be taken of the monodentancy of both acrylate anions in the case of copper as a complexing agent with coordination number 5, noted in our previous work.[32] Apparently, such difference in the dentacy of acrylates is related to the size of the metal cations of the complexing agents.

Also of note is the similarity of spatial environment of the metal ion with that of analogous bipyridine complexes with nickel and copper acrylates, in which metal ions were six-coordinated and acid anions were coordinated differently, whereas, *e.g.*, the zinc ion coordinated both acid anions bidentatively (Table S6).[33] The same double bidentate coordination of acrylate anions is also shown by the complex of copper acrylate with di(2-pyridyl)amine.[34] It is probable that the observed difference in the type of coordination is related to the type of ligand and synthesis conditions.

The difference in the length of metal–nitrogen bonds in cases of coordination of one or two terpyridine ligands is also of interest. The classical coordination of a metal to a ligand leads to the formation of bis-terpyridine clusters. When the terpyridine derivative is coordinated with a metal acrylate, the metal–nitrogen bond lengths would decrease (see Table S6).[35] This fact may also have a beneficial effect on the self-healing of the polymers derived from such complexes due to the enhanced coordination interactions.

hydrogen atoms were refined with anisotropic displacement parameters. All hydrogen atoms were refined isotropically on calculated positions using a riding model with their U_{iso} values constrained to 1.5 times the U_{eq} of their pivot atoms for terminal sp^3 carbon atoms and 1.2 times for all other carbon atoms. Disordered moieties were refined using bond lengths restraints and displacement parameter restraints. This report and the CIF file were generated using FinalCif.[31]

CCDC 2338563 contains the supplementary crystallographic data for this paper. These data can be obtained free of charge from The Cambridge Crystallographic Data Centre *via* http://www.ccdc.cam.ac.uk.

The results of elemental analysis of the herein obtained complex $NiAcr_2PhTpy$ (Table S7) are close to the theory. The main characteristic bands analysis of the IR spectrum of $NiAcr_2PhTpy$ (Figure S1) was carried out in accordance with data.[36] The intense absorption bands at 3550–3300 cm^{-1} probably indicate the intermolecular hydrogen bonds presence due to the small amount of solvent molecules in the monomer; vibrations in the region of 3060 cm^{-1} refer to the C–H vibrations of the pyridine rings. The peak at 1637 cm^{-1} relates to the C=C bond and the peaks at 1557 and 1415 cm^{-1} correspond to the asymmetric and symmetric vibrations of the COO^- acrylic acid ion; the symmetric vibration band is shifted to a lower frequency region relative to the COO^- vibration of nickel acrylate (1440 cm^{-1}) apparently due to coordination with terpyridine. The 1603 and 1570 cm^{-1} peaks correspond to the skeletal vibrations of the pyridine rings, and 1613 cm^{-1} to the C=N vibrations. The =C–H bond deformation vibration band characteristic of monosubstituted benzenes is observed at 770 cm^{-1}, as for the spectrum of the very terpyridine.[37] The peaks in the 660–680 cm^{-1} region can be attributed to M–O vibrations. It is important to mention the shift of the 1040 cm^{-1} peak of the pyridine rings strain vibrations in the free ligand to 1017 cm^{-1} (inset in Figure S1), which is caused by the Lewis acid-type coordination of the terpyridine.[38]

In the absorption spectrum of $NiAcr_2PhTpy$ in UV and visible ranges (Figure S2), attention should be paid to the absorption band in the region of 430 nm related to the metal–ligand charge transfer and absent in the spectrum of phenylterpyridine, which indicates successful complexation.

The thermal studies results are summarized in Figure 2 and Table S8. The decomposition proceeds in four steps according to the TGA curve. The first step occurs up to 275 °C and is due to dehydration, and a region of loss of physically adsorbed water molecules up to 120 °C can be distinguished. The second step is observed at 280–300 °C and is characterized by the highest decomposition rate and maximum exothermic effect (133 J g^{-1}), indicating solid-phase monomer polymerization conjugated with decarboxylation processes. Second stage mass loss can be attributed to both outgassing and the beginning of phenylterpyridine decomposition, determining a different decomposition character at the third stage in the 300–380 °C region. Complete decarboxylation and decomposition of the obtained metallopolymer to the metal-containing phase is observed in the last fourth step.

The phenylterpyridine thermal behavior was also investigated to clarify the decomposition mechanism of the metallocomplex (Figure S3). There are two endothermic peaks on the DSC curve, the first belongs to the melting process (210 °C). The second peak with a minimum at 350 °C corresponds to the decomposition process accompanied by complete mass loss. Probably, the endothermic melting peak of phenylterpyridine at 210 °C is shifted to 260 °C for the obtained complex (see Figure 2), which

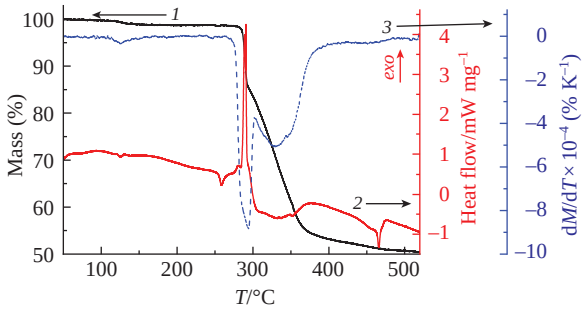

Figure 2 (*1*) TGA, (*2*) DSC and (*3*) DTG curves of $NiAcr_2PhTpy$ (heating rate is 10 K min^{-1}).

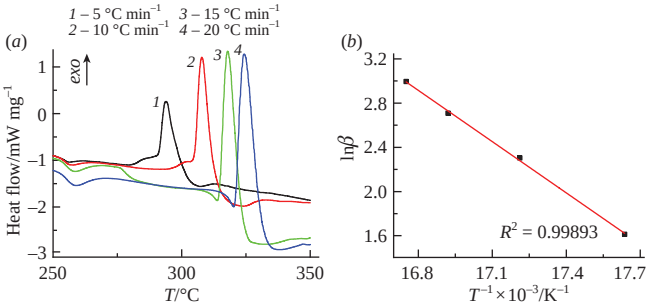

Figure 3 (*a*) DSC curves of $NiAcr_2PhTpy$ at different heating rates; (*b*) Arrhenius dependence of the heating rate logarithm on the inverse temperature.

may indicate the breaking of metal–ligand coordination bonds. Then solid-phase polymerization and outgassing reactions begin, causing a different slope from the phenylterpyridine decomposition region (see Figure S3) at 280–300 °C on the TGA curves of the metal complex (see Figure 2).

DSC data were obtained at different heating temperature rates to estimate the effective activation energy of solid-phase polymerization [Figure 3(*a*)]. The dependence of the heating rate logarithm on the temperature of the exothermic peak maximum of solid-phase polymerization was plotted in $\ln\beta - 1/T$ coordinates in accordance with ASTM E698 [Figure 3(*b*)].[39]

The effective activation energy of solid-phase polymerization $E_a \approx 129 \pm 2$ kJ mol^{-1} was calculated (see Online Supplementary Materials) based on the obtained data. It was not possible to compare the activation energy calculated by DSC with the analysis by TGA due to the co-occurrence of polymerization and decomposition of terpyridine fragment. However, the obtained activation energy value is close to the values determined for similar nickel complexes.[40]

Thus, a new metallocomplex based on nickel acrylate and 4′-phenyl-2,2′:6′,2′-terpyridine for further preparation of self-healing metallopolymers based on it was obtained and characterized. The X-ray diffraction analysis reveals that the complex possesses a primitive triclinic lattice, where the coordination number of Ni^{II} is 6. The presented heat of opening of double bonds and activation energy of solid-phase polymerization, along with structural parameters, may affect the final composition, structure and properties of self-healing polymers.

This work has been carried out in accordance with the state tasks (registration nos. 124013000757-0, 124013000722-8 and 124013100858-3) using the equipment of the Federal Research Center of Problems of Chemical Physics and Medicinal Chemistry RAS.

Online Supplementary Materials

Supplementary data associated with this article can be found in the online version at doi: 10.1016/j.mencom.2024.04.022.

References

1 Y. Bai, C. Zhang, C. Xu and C. Yan, *Front. Chem. China*, 2010, **5**, 123.
2 R. G. De Lima, M. G. Sauaia, C. Ferezin, I. M. Pepe, N. M. José, L. M. Bendhack, Z. N. Da Rocha and R. S. Da Silva, *Polyhedron*, 2007, **26**, 4620.
3 Z.-Q. Liang, C.-X. Wang, J.-X. Yang, H.-W. Gao, Y.-P. Tian, X.-T. Tao and M.-H. Jiang, *New J. Chem.*, 2007, **31**, 906.
4 U. Resch-Genger, Y. Q. Li, J. L. Bricks, V. Kharlanov and W. Rettig, *J. Phys. Chem. A*, 2006, **110**, 10956.
5 J. R. Peterson, T. A. Smith and P. Thordarson, *Org. Biomol. Chem.*, 2010, **8**, 151.
6 M. Savic, A. Arsenijevic, J. Milovanovic, B. Stojanovic, V. Stankovic, A. Rilak Simovic, D. Lazic, N. Arsenijevic and M. Milovanovic, *Molecules*, 2020, **25**, 4699.
7 M. Gil-Moles, M. E. Olmos, M. Monge, M. Beltrán-Visiedo, I. Marzo, J. M. López-de-Luzuriaga and M. C. Gimeno, *Chem. – Eur. J.*, 2023, **29**, e202300116.
8 Q.-P. Qin, Z.-F. Wang, S.-L. Wang, D.-M. Luo, B.-Q. Zou, P.-F. Yao, M.-X. Tan and H. Liang, *Eur. J. Med. Chem.*, 2019, **170**, 195.
9 C. Li, F. Xu, Y. Zhao, W. Zheng, W. Zeng, Q. Luo, Z. Wang, K. Wu, J. Du and F. Wang, *Front. Chem.*, 2020, **8**, 210.
10 J. Li, M. Chen, J. Jiang, J. Huang, H. Chen, L. Pan, D. S. Nesterov, Z. Ma and A. J. L. Pombeiro, *Int. J. Mol. Sci.*, 2023, **24**, 3903.
11 F. Yu. Vyalba, A. V. Ivantsova, K. A. Zhdanova, M. N. Usachev, M. A. Gradova and N. A. Bragina, *Mendeleev Commun.*, 2022, **32**, 675.
12 B. Liu, Y. Gao, M. A. Jabed, S. Kilina, G. Liu and W. Sun, *ACS Appl. Bio Mater.*, 2020, **3**, 6025.
13 X. Guo, M. Bian, F. Lv, Y. Wang, Z. Zhao, Z. Bian, B. Qu, L. Xiao and Z. Chen, *J. Mater. Chem. C*, 2019, **7**, 11581.
14 X. Guo, Z. Tang, W. Yu, Y. Wang, Z. Zhao, J. Gu, Z. Liu, B. Qu, L. Xiao and Z. Chen, *Org. Electron.*, 2021, **89**, 106048.
15 B. Nemati Bideh, H. Shahroosvand, A. Sousaraei and J. Cabanillas-Gonzalez, *Sci. Rep.*, 2019, **9**, 228.
16 M.-H. Zhou, J.-Y. Lin, W.-P. Zhang, J.-X. Jian, F. W. Dagnaw, T. Wang and Q.-X. Tong, *Solar RRL*, 2023, **7**, 2201018.
17 I. L. Mallphanov and V. K. Vanag, *Mendeleev Commun.*, 2022, **32**, 507.
18 M. Mauro, *Eur. J. Inorg. Chem.*, 2018, 2090.
19 K. C. Bentz and S. M. Cohen, *Angew. Chem., Int. Ed.*, 2018, **57**, 14992.
20 A. Levy, R. Feinstein and C. E. Diesendruck, *J. Am. Chem. Soc.*, 2019, **141**, 7256.
21 L. Arnedo-Sánchez, Nonappa, S. Bhowmik, S. Hietala, R. Puttreddy, M. Lahtinen, L. De Cola and K. Rissanen, *Dalton Trans.*, 2017, **46**, 7309.
22 E. Borré, J.-F. Stumbé, S. Bellemin-Laponnaz and M. Mauro, *Chem. Commun.*, 2017, **53**, 8344.
23 E. Borré, J. Stumbé, S. Bellemin-Laponnaz and M. Mauro, *Angew. Chem., Int. Ed.*, 2016, **55**, 1313.
24 R. K. Baimuratova, G. I. Dzhardimalieva, E. V. Vaganov, V. A. Lesnichaya, G. D. Kugabaeva, K. A. Kydralieva, V. A. Zhinzhilo and I. E. Uflyand, *Polymers*, 2021, **13**, 1760.
25 E. S. Sorin, R. K. Baimuratova, D. A. Chernyayev, D. V. Korchagin, I. E. Uflyand and G. I. Dzhardimalieva, *Key Eng. Mater.*, 2021, **899**, 37.
26 E. S. Sorin, R. K. Baimuratova, I. E. Uflyand, E. O. Perepelitsina, D. V. Anokhin, D. A. Ivanov and G. I. Dzhardimalieva, *Polymers*, 2023, **15**, 1472.
27 *CrysAlisPRO*, Agilent Technologies UK Ltd., Yarnton, England, 2011.
28 G. M. Sheldrick, *Acta Crystallogr., Sect. A: Found. Adv.*, 2015, **71**, 3.
29 G. M. Sheldrick, *Acta Crystallogr., Sect. C: Struct. Chem.*, 2015, **71**, 3.
30 O. V. Dolomanov, L. J. Bourhis, R. J. Gildea, J. A. K. Howard and H. Puschmann, *J. Appl. Crystallogr.*, 2009, **42**, 339.
31 D. Kratzert, *FinalCif*, v134, https://dkratzert.de/finalcif.html.
32 I. E. Uflyand, V. V. Tkachev, V. A. Zhinzhilo, E. G. Drogan, V. E. Burlakova, M. E. Sokolov, V. T. Panyushkin, R. K. Baimuratova and G. I. Dzhardimalieva, *J. Mol. Struct.*, 2022, **1250**, 131909.
33 G. V. Scăeţeanu, M. C. Chifiriuc, C. Bleotu, C. Kamerzan, L. Măruţescu, C. G. Daniliuc, C. Maxim, L. Calu, R. Olar and M. Badea, *Molecules*, 2018, **23**, 157.
34 P. Liu, C.-J. Wang, Y.-Y. Wang, W.-L. Qin, R. Sun, D.-S. Li and Q.-Z. Shi, *J. Coord. Chem.*, 2006, **59**, 729.
35 N. Zhang, J. Yang, R.-X. Hu and M.-B. Zhang, *Z. Anorg. Allg. Chem.*, 2013, **639**, 197.
36 G. Socrates, *Infrared and Raman Characteristic Group Frequencies: Tables and Charts*, 3rd edn., Wiley, Chichester, 2001.
37 *PubChem Compound Summary for CID 70848, 2,2':6',2''-Terpyridine*. https://pubchem.ncbi.nlm.nih.gov/compound/2_6-dipyridin-2-ylpyridine.
38 H. Yamada and Y. Yamamoto, *J. Chem. Soc.*, 1979, **75**, 1215.
39 *Standard Test Method for Arrhenius Kinetic Constants for Thermally Unstable Materials Using Differential Scanning Calorimetry and the Flynn/Wall/Ozawa Method*, ASTM International, E27 Committee.
40 V. A. Zhinzhilo, *PhD Thesis*, 2020.

Received: 29th December 2023; Com. 23/7356